Simulation of light scattering in large, disordered nanostructures using a periodic T-matrix method

Dominik Theobald[a,*], Dominik Beutel[b], Luisa Borgmann[c], Henning Mescher[a,c], Guillaume Gomard[a,c], Carsten Rockstuhl[b,d], Uli Lemmer[a,c]

[a]*Light Technology Institute (LTI), Karlsruhe Institute of Technology (KIT), Kaiserstrasse 12, 76131 Karlsruhe, Germany*
[b]*Institut für Theoretische Festkörperphysik (TFP), Karlsruhe Institute of Technology (KIT), Kaiserstrasse 12, 76131 Karlsruhe, Germany*
[c]*Institute of Microstructure Technology (IMT), Karlsruhe Institute of Technology (KIT), Hermann-von-Helmholtz-Platz 1, 76344 Eggenstein-Leopoldshafen, Germany*
[d]*Institute of Nanotechnology (INT), Karlsruhe Institute of Technology (KIT), Hermann-von-Helmholtz-Platz 1, 76344 Eggenstein-Leopoldshafen, Germany*

Abstract

To model and design light propagation in disordered optical nanostructures and materials, any applicable simulation technique has to cope with enormous computational challenges in a bearable time frame. To circumvent these, the introduction of an artificial periodicity to the disordered particle structure allows to rely on computational techniques that exploit periodic boundary conditions. Choosing a rather large periodicity promises to preserve randomness in form of a close-range disorder but can introduce false interferences. So far, it remains open how the artificial periodicity has to be chosen to minimize its detrimental influence. Here, we combine the superposition T-matrix scheme with an Ewald sum formulation to account for light scattering in periodic particle arrangements that contain hundreds to thousands of individual scatterers per unit cell. Simulations reveal that the periodicity's influence cannot be minimized by simply choosing one single period much longer than the excitation wavelength. The excitation of lattice induced resonances prevents so. However, choosing a periodicity that does not sustain such detrimental features allows for reliable predictions. With that, the presented approach is suitable to derive spectral information about wave-optical phenomena in large, random particle arrangements with a spatial extend beyond those accessible with other full-wave solvers.

Keywords: Multiple scattering, T-matrix method, Ewald summation, Disordered media, Artificial periodicity

1. Introduction

With growing awareness of disorder in natural photonic structures [1, 2, 3], a strong desire emerges to study, mimic and design materials that can be used, e.g., to create structural colors [4, 5], manage light propagation in organic light emitting devices [6, 7], improve light harvesting in thin film solar cells [8, 9] or provide interesting properties in form of metamaterials [10, 11]. The disparity of involved length scales, with features on a nano-scale and device characteristics possibly on a centimeter- or meter-scale, renders the quantitative description of the emerging phenomena extremely challenging. In this context, the superposition T-matrix scheme [12, 13] enjoys great popularity as one of the most powerful tools for the description of wave-optical phenomena in large particle configurations. Its computational effort does not scale directly with the size of the simulation domain but rather with the number and size of involved scatterers. As the scattering of each individual nanoparticle is described semi-analytically, the approach can draw a major advantage over the more established numerical simulation techniques, like the finite element method (FEM) or the finite-difference time-domain method (FDTD) that have been utilized for extensive studies within this field [14, 15].

Although the superposition T-matrix approach can handle large, random particle arrangements comprising tens of thousands of individual scatterers [16, 17], its complexity of $\mathcal{O}(N^2)$ or at least $\mathcal{O}(Nlog(N))$ [18] scales with the particle count and raises unavoidable challenges in terms of computational resources and time.

When individual simulations start to tax our patience, parameter studies become unfeasible and the quantitative design of disorder gets out of reach. In this context, it can be of interest to approximate spatially extended random particle arrangements by introducing a rather large artificial periodicity. The general assumption is that the random nature of the particle arrangement can be preserved thanks to the short-range disorder within one unit cell, while the detrimental influence of the periodicity is kept at a minimum by considering unit cells much larger than the wavelength of interest, often called supercells. As

---

*Corresponding author
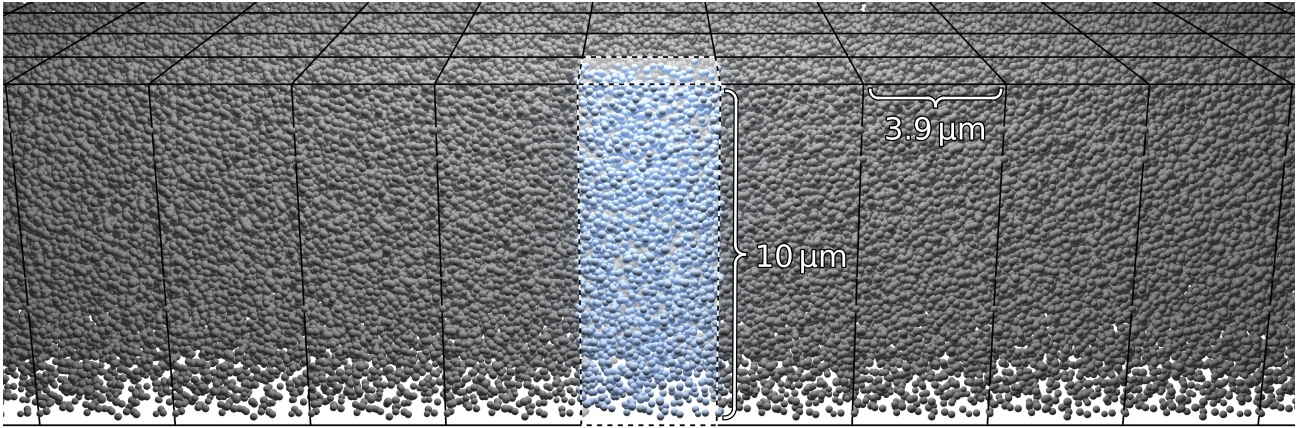
Figure 1: Illustration of a random particle arrangement with an artificial two-dimensional periodicity of 3.9 μm and a height of 10 μm. With a volume density of 7 % (v/v), the exemplary configuration consists of more than 2000 individual nanoparticles per unit cell.

a result, one can capitalize on computational tools that explicitly exploit the periodicity in their solution strategy to Maxwell's equations.

Seeking the optical response of small, disordered metal inclusions in dielectric host media, Lamb *et al.* [19] and Liebsch *et al.* [20] extended effective medium approximations by mimicking disorder with a periodic, average scattering response. Soon, early T-matrix formalisms emerged utilizing the average T-matrix approximation [21] or the coherent potential approximation [22, 23] to average the scattering response of such a unit cell. Since then, T-matrix schemes for the optical response of particle arrays have been presented, e.g., by Stefanou *et al.* [24, 25] and recently, by Beutel *et al.* [26] and Nečada *et al.* [27], utilizing Kambe's Ewald sum formulation for spherical vector wave functions (SVWFs) [28, 29]. Besides the multipole approach, comparable strategies on the basis of the discrete dipole approximation (DDA) have been applied to periodic particle arrangements [30, 31] allowing to investigate optical properties of inhomogeneous media [32, 33].

In this contribution, we adapt the Ewald sum approach to perform T-matrix simulations of light scattering by large, three-dimensional unit cells of two-dimensional periodicity, containing hundreds to thousands of disordered particles (illustrated in figure 1). In section 2, we summarize the integration of Ewald's method into the superposition T-matrix scheme. To emphasize the use of the presented approach, we compare simulations of a $2 \times 2 \times 2 \, \mu m^3$ large unit cell to the well-established FEM in section 3 and elaborate on the use of periodic boundary conditions to mimic disorder. In section 4, we treat a specific example of wavelength dependent reflection of light by 10 μm thick porous polymer layers. Such polymer matrices that incorporate nano- to micro-sized air bubbles have received increasing attention as a possible substitute of white pigments, such as TiO_2 nanoparticles. TiO_2, widely used in plastic packaging, coatings and paints, raises an increasing number

of concerns regarding material costs, eco-friendliness and health issues [34]. In contrast, pigment-free polymer foams present themselves as an inexpensive and easily recyclable alternative for flexible, yet mechanically stable packaging for food and cosmetics without drawbacks in white appearance [35].

Porous polymer structures can be formed by supercritical CO_2 foaming. In this process, the polymer is first saturated with CO_2 under constant pressure and temperature. With increasing CO_2 concentration, the polymer's glass transition temperature decreases and the polymer becomes viscous. A sudden pressure drop causes a supersaturation of CO_2 in the polymer host and nucleation occurs. Under these conditions, the CO_2 is not soluble in the polymer matrix anymore. It escapes into the nuclei that thus grow into pores. Due to the thereby decreasing CO_2 concentration, the polymer's glass transition temperature rises again and the matrix solidifies [36]. Pore size and density can be controlled by pressure and temperature.

2. T-matrix procedure

The superposition T-matrix method allows to describe electromagnetic scattering in particle ensembles. To highlight the integration of periodic boundary conditions, we first summarize its general procedure. For comprehensive descriptions please see, e.g., Refs. [37, 38].

In the picture of a multipole decomposition of waves, a particle's incoming and scattered time-harmonic electric field can be expressed in regular and outgoing spherical vector wave functions $\mathbf{M}_n^{(1)}(\mathbf{r})$ and $\mathbf{M}_n^{(3)}(\mathbf{r})$ (cf. Appendix A),

$$\mathbf{E}(\mathbf{r}) = \mathbf{E}_{in}(\mathbf{r}) + \mathbf{E}_{sca}(\mathbf{r})$$
$$= \sum_n a_n \mathbf{M}_n^{(1)}(\mathbf{r}) + b_n \mathbf{M}_n^{(3)}(\mathbf{r}). \quad (1)$$

For a simpler notation, the multi index n subsumes a multipole's degree l, order m and polarization τ, $(lm\tau) \to n$. A particle's T-matrix maps the amplitudes of the incoming field to its scattered field

$$b_n = \sum_{n'} T_{nn'} a_{n'}. \tag{2}$$

This linear operator contains all information about the scatterer and throughout this work we assume that each particle's T-matrix is precisely known. For spherical particles, the diagonal T-matrix is identical to the Mie coefficients and for more complex objects a variety of numerical techniques are available [39, 40, 41].

In the presence of multiple scatterers, the incoming field of particle S depends on the initial field and the scattered fields of all other particles S'

$$a_n^S = a_n^{S,\text{init}} + \sum_{S'} \sum_{n'} W_{nn'}^{SS'} b_{n'}^{S'}. \tag{3}$$

Inserting (3) into (2) yields a self-consistent set of linear equations to account for multiple scattering

$$b_n^S - \sum_{n'} T_{nn'}^S \sum_{S'} \sum_{n''} W_{n'n''}^{SS'} b_{n''}^{S'} = \sum_{n'} T_{nn'}^S a_{n'}^{S,\text{init}}. \tag{4}$$

Neglecting indirect coupling, e.g. via layer interfaces, the coupling operator W can be expressed as the transpose of the translation addition operator for SVWFs (cf. eq. (A.6))

$$W_{nn'}^{SS'} = A_{n'n} \left(\mathbf{r}_S - \mathbf{r}_{S'} \right). \tag{5}$$

2.1. Periodicity

Considering three-dimensional, periodic particle arrangements in a two-dimensional Bravais lattice, we distinguish between the q-th particle S_{pq} in unit cell p and periodic particle collection S_q of all q-th particles ($q = q'$). In collection S_q any particle displacement $\mathbf{r}_{S_{p'q}} - \mathbf{r}_{S_{0q}} = n_1 \mathbf{a}_1 + n_2 \mathbf{a}_2 = \mathbf{R}_{p'}$ coincides with a linear combination of the lattice vectors $\mathbf{a}_1$ and $\mathbf{a}_2$, with n_1, $n_2 \in \mathbb{Z}$ specifying unit cell $(n_1, n_2) \to p'$.

Excited by a plane wave, the initial incoming field of particles in collection S_q resemble each other but exhibit a phase shift

$$a_n^{S_{p'q},\text{init}} = e^{i\mathbf{k}_{\text{in}||}(\mathbf{r}_{S_{p'q}} - \mathbf{r}_{S_{0q}})} a_n^{S_{0q},\text{init}} = e^{i\mathbf{k}_{\text{in}||}\mathbf{R}_{p'}} a_n^{S_{0q},\text{init}}, \tag{6}$$

based on the initial field's in-plane wave vector $\mathbf{k}_{\text{in}||}$ and the particles' displacement. According to the Bloch theorem, the quasi-periodicity of the right-hand side of (6) demands for the same quasi-periodicity in the solution of (4). Hence, a particle collection's scattered fields satisfy

$$b_n^{S_{p'q}} = e^{i\mathbf{k}_{\text{in}||}\mathbf{R}_{p'}} b_n^{S_{0q}}, \tag{7}$$

reducing the number of unknowns to the scattered field amplitudes of particles within one unit cell. Inserting (7)

into (4), with $S = S_{0q}$ and $S' = S_{p'q}$, the linear set of equations of particles in the arbitrary central unit cell ($p = 0$) reads

$$b_n^{S_{0q}} - \sum_{n'} T_{nn'}^{S_{0q}} \sum_{p'} \sum_{q'} \sum_{n''} W_{n'n''}^{S_{0q}S_{p'q'}} b_{n''}^{S_{p'q'}} = \sum_{n'} T_{nn'}^{S_{0q}} a_{n'}^{S_{0q},\text{init}}. \tag{8}$$

In contrast to the conventional superposition T-matrix method, its central concern being particle-particle coupling, the periodicity raises the question of how periodic particle grids couple to each other.

Recalling the translation addition operator (eqs. (A.8) and (A.9)), the infinite sum of particle-particle coupling in (8) between all q-th particles in collection S_q can be written as

$$\sum_{p'} W_{nn'}^{S_{0q}S_{p'q}} e^{i\mathbf{k}_{\text{in}||}\left(\mathbf{r}_{S_{p'q}} - \mathbf{r}_{S_{0q}}\right)}$$

$$= \sum_{p' \neq 0} A_{n'n}(-\mathbf{R}_{p'}) e^{i\mathbf{k}_{\text{in}||}\mathbf{R}_{p'}}$$

$$= \sum_{L=|l-l'|}^{|l+l'|} \begin{cases} a_5(l', m'|l, m|L) \\ b_5(l', m'|l, m|L) \end{cases}$$

$$\times \sum_{p' \neq 0} h_L^{(1)}(k|\mathbf{R}_{p'}|) Y_{LM}(-\mathbf{R}_{p'}) e^{i\mathbf{k}_{\text{in}||}\mathbf{R}_{p'}} \quad \begin{matrix} \tau = \tau' \\ \tau \neq \tau'. \end{matrix} \tag{9}$$

Here, $h_l^{(1)}$ denotes the spherical Hankel function of first kind, $Y_{lm}(\theta, \varphi)$ the spherical harmonics and $M = m' - m$. Due to slow convergence of the inner sum in (9), its numerical evaluation can be challenging. However, the sum is identical to the structure coefficients D_{LM} in low energy electron diffraction theory [42]

$$D_{LM}(\mathbf{R}_{p'}) = \sum_{p' \neq 0} h_L^{(1)}(k|\mathbf{R}_{p'}|) Y_{LM}(-\mathbf{R}_{p'}) e^{i\mathbf{k}_{\text{in}||}\mathbf{R}_{p'}}. \tag{10}$$

Making use of Ewald's method, the evaluation of D_{LM} can be split in two equally fast converging sums, as derived by Kambe [28, 29] in the case of a two dimensional lattice. Explicit formulas for D_{LM} can be found in Appendix B.

2.2. Scattered field

Due to the nature of infinite periodic lattices, the particles' scattered field has an infinite number of source terms, rendering the direct evaluation challenging. We start with the scattered field of particle collection S_q as a sum of each particle's outgoing SVWFs $\mathbf{M}_n^{(3)}$

$$\mathbf{E}_{\text{sca}}^{S_q}(\mathbf{r}) = \sum_p \sum_n b_n^{S_{pq}} \mathbf{M}_n^{(3)}\left(\mathbf{r} - \mathbf{r}_{S_{pq}}\right)$$

$$= \sum_{p'} \sum_n b_n^{S_{0q}} e^{i\mathbf{k}_{\text{in}||}\mathbf{R}_{p'}} \mathbf{M}_n^{(3)}(\mathbf{r} - \mathbf{r}_{S_{0q}} - \mathbf{R}_{p'}). \tag{11}$$

3

Utilizing the SVWFs' integral representation (A.5) we obtain

$$\mathbf{E}_{\text{sca}}^{S_q}(\mathbf{r}) = \frac{1}{2\pi} \sum_{p'} \sum_n b_n^{S_{0q}} \sum_{j=1}^2 \int \frac{d^2\mathbf{k}_{||}}{k_z k} e^{im\alpha}$$
$$\times B_{nj}\left(\pm\frac{k_z}{k}\right) e^{i\mathbf{k}^\pm(\mathbf{r}-\mathbf{r}_{S_{0q}})} e^{i(\mathbf{k}_{\text{in}||}-\mathbf{k}^\pm)\mathbf{R}_{p'}} \hat{\mathbf{e}}_j^\pm. \tag{12}$$

Here, $\kappa, \alpha, \pm k_z$ denote the cylindrical coordinates of wave vector $\mathbf{k}^\pm$. Dependent on the relative position of $\mathbf{r}$, the plus and minus sign correspond to upwards $(+)$ or downwards $(-)$ propagating plane waves that have to be taken into account.

Introducing the linear combination of reciprocal lattice vectors $\mathbf{b}_1$ and $\mathbf{b}_2$, $\mathbf{G}_{\tilde{p}} = m_1\mathbf{b}_1 + m_2\mathbf{b}_2$, with $m_1, m_2 \in \mathbb{Z}$ specifying unit cell $(m_1, m_2) \to \tilde{p}$, and making use of the Poisson summation formula

$$\sum_{p'} e^{i(\mathbf{k}_{\text{in}||}-\mathbf{k}^\pm)\mathbf{R}_{p'}} = \frac{(2\pi)^2}{A_{\text{uc}}} \sum_{\tilde{p}} \delta(\mathbf{k}^\pm - \mathbf{k}_{\text{in}||} + \mathbf{G}_{\tilde{p}}), \tag{13}$$

we find the scattered field of particle collection S_q written as a sum of discrete plane waves

$$\mathbf{E}_{\text{sca}}^{S_q}(\mathbf{r}) = \sum_{j=1}^2 \sum_{\tilde{p}} g_{S_{0q},j}^\pm(\kappa, \alpha) \boldsymbol{\Phi}_j^\pm(\kappa, \alpha; \mathbf{r} - \mathbf{r}_{S_{0q}})$$
$$\times \delta(\mathbf{k}^\pm - \mathbf{k}_{\text{in}||} + \mathbf{G}_{\tilde{p}}) \tag{14}$$

with amplitudes

$$g_{S_{0q},j}^\pm(\kappa, \alpha) = \frac{2\pi}{A_{\text{uc}}} \sum_n b_n^{S_{0q}} \frac{1}{k_z k} e^{im\alpha} B_{nj}\left(\pm\frac{k_z}{k}\right). \tag{15}$$

A_{uc} denotes one unit cell's base area and $\boldsymbol{\Phi}^\pm$ the upwards or downwards oriented plane vector wave functions (cf. eq. (A.1)). For practical reasons, the infinite sum in (14) over scattered wave vectors $\mathbf{k}^\pm = \mathbf{k}_{\text{in}||} - \mathbf{G}_{\tilde{p}}$ has to be truncated at a finite order of $\tilde{p} < \tilde{p}_{\text{max}}$. Note that the reciprocal lattice vectors can be constructed from their real space counterparts, $\mathbf{b}_1 = 2\pi R_{\pi/2}\mathbf{a}_2/(\mathbf{a}_1 \cdot R_{\pi/2}\mathbf{a}_2)$ and $\mathbf{b}_2 = 2\pi R_{\pi/2}\mathbf{a}_1/(\mathbf{a}_2 \cdot R_{\pi/2}\mathbf{a}_1)$ with rotation matrix R_α of angle α. Hereby, the lattice vectors satisfy $\mathbf{a}_i \cdot \mathbf{b}_j = 2\pi\delta_{ij}$ and $\mathbf{R}_{p'} \cdot \mathbf{G}_{\tilde{p}} = 2\pi N$ for some integer N.

2.3. Scattered far-field

Besides the scattered near-field, the discrete sum (14) of propagating ($\kappa \leq k$) and evanescent ($\kappa > k$) plane waves allows to determine far-field properties like the angle dependent transmittance and reflectance.

The power per area each plane wave carries into z direction reads

$$I_A^\pm = \frac{dP}{dA} = \frac{k}{2\omega\mu_0} \cos\beta^\pm |g^\pm(\kappa, \alpha)|^2. \tag{16}$$

ω denotes the angular frequency, μ_0 the free space permeability and β the polar angle of propagation. For upwards

propagating plane waves $\beta^+ = \arcsin(\kappa/k)$ and for downwards propagating plane waves $\beta^- = \pi - \arcsin(\kappa/k)$.

The sum over all scattered, propagating plane waves yields the total transmitted and reflected power per area of a periodic particle arrangement

$$I^\pm = \frac{k}{2\omega\mu_0} \sum_q \sum_{j=1}^2 \sum_{\tilde{p}} \cos\beta |g_{S_{0q},j}^\pm(\kappa, \alpha)|^2$$
$$\times \delta(\mathbf{k}^\pm - \mathbf{k}_{\text{in}||} + \mathbf{G}_{\tilde{p}}), \qquad |\mathbf{k}^\pm| \leq k. \tag{17}$$

Since all particles in a unit cell share the same periodicity, each particle collection scatters into the same discrete plane waves. As a result, the far-field's angular distribution is not continuous. However, with growing unit cell size the reciprocal lattice vectors decrease, resulting in an increasing number of propagating plane waves. In the limit of lattice vectors of infinite size, the scattered far-field distribution becomes continuous.

2.4. Direct plane wave coupling

Comparable to nonspherical particles with overlapping circumscribing spheres, the coupling between particle collections S_q and $S_{q'}$ can be ev

Given that particle collections S_q and $S_{q'}$ can be separated by a plane parallel to the xy plane

$$z_{S_{0q}} - z_{S_{0q'}} = \Delta z_{S_q S_{q'}} > r_{S_{0q}} - r_{S_{0q'}} \tag{18}$$

it can be advantageous to evaluate the particle-grid coupling in terms of plane waves instead of using Ewald summation. Such a configuration is comparable to nonspherical particles with overlapping circumscribing spheres, for which a reformulation of the translation addition operator in form of plane waves can be applied [43].

We start with a translation of the scattered field of particle collection $S_{q'}$ (14) to the center of particle S_{0q}

$$\mathbf{E}_{\text{sca}}^{S_{q'}}(\mathbf{r}) = \frac{2\pi}{A_{\text{uc}}} \sum_{n'} b_{n'}^{S_{0q'}} \sum_{j=1}^2 \sum_{\tilde{p}} \frac{1}{k_z k} e^{im'\alpha} B_{n'j}\left(\pm\frac{k_z}{k}\right)$$
$$\times \boldsymbol{\Phi}_j^\pm(\kappa, \alpha; \mathbf{r} - \mathbf{r}_{S_{0q'}}) \delta(\mathbf{k}^\pm - \mathbf{k}_{\text{in}||} + \mathbf{G}_{\tilde{p}})$$
$$= \frac{2\pi}{A_{\text{uc}}} \sum_{n'} b_{n'}^{S_{0q'}} \sum_{j=1}^2 \sum_{\tilde{p}} \frac{1}{k_z k} e^{im'\alpha} B_{n'j}\left(\pm\frac{k_z}{k}\right)$$
$$\times e^{i\mathbf{k}^\pm(\mathbf{r}_{S_{0q}}-\mathbf{r}_{S_{0q'}})} \boldsymbol{\Phi}_j^\pm(\kappa, \alpha; \mathbf{r} - \mathbf{r}_{S_{0q}})$$
$$\times \delta(\mathbf{k}^\pm - \mathbf{k}_{\text{in}||} + \mathbf{G}_{\tilde{p}}). \tag{19}$$

Now, a transformation into regular SVWFs (A.4)

$$\mathbf{E}_{\text{sca}}^{S_{q'}}(\mathbf{r}) = \frac{8\pi}{A_{\text{uc}}} \sum_n \sum_{n'} b_{n'}^{S_{0q'}} \sum_{j=1}^2 \sum_{\tilde{p}} \frac{1}{k_z k} e^{i(m'-m)\alpha}$$
$$\times B_{n'j}\left(\pm\frac{k_z}{k}\right) B_{nj}^\dagger\left(\pm\frac{k_z}{k}\right) e^{i\mathbf{k}^\pm(\mathbf{r}_{S_{0q}}-\mathbf{r}_{S_{0q'}})}$$
$$\times \mathbf{M}_n^{(1)}(\mathbf{r} - \mathbf{r}_{S_{0q}}) \delta(\mathbf{k}^\pm - \mathbf{k}_{\text{in}||} + \mathbf{G}_{\tilde{p}}) \tag{20}$$

yields the incoming field coefficients of particle S_{0q} that directly originate from the scattered field of particle collection $S_{q'}$

$$a_n^{S_{0q}S_{q'}} = \sum_{n'} W_{nn'}^{S_{0q}S_{q'}} b_{n'}^{S_{0q'}},$$

$$= \frac{8\pi}{A_{\mathrm{uc}}} \sum_{n'} b_{n'}^{S_{0q'}} \sum_{j=1}^{2} \sum_{\tilde{p}} \frac{1}{k_z k} \mathrm{e}^{\mathrm{i}(m'-m)\alpha}$$

$$\times B_{n'j}\left(\pm \frac{k_z}{k}\right) B_{nj}^{\dagger}\left(\pm \frac{k_z}{k}\right) \mathrm{e}^{\mathrm{i}\mathbf{k}^{\pm}(\mathbf{r}_{S_{0q}}-\mathbf{r}_{S_{0q'}})}$$

$$\times \delta(\mathbf{k}^{\pm} - \mathbf{k}_{\mathrm{in}||} + \mathbf{G}_{\tilde{p}}) \tag{21}$$

and the coupling operator

$$W_{nn'}^{S_{0q}S_{q'}} = \frac{8\pi}{A_{\mathrm{uc}}} \sum_{j=1}^{2} \sum_{\tilde{p}} \frac{1}{k_z k} \mathrm{e}^{\mathrm{i}(m'-m)\alpha}$$

$$\times B_{n'j}\left(\pm \frac{k_z}{k}\right) B_{nj}^{\dagger}\left(\pm \frac{k_z}{k}\right) \mathrm{e}^{\mathrm{i}\mathbf{k}^{\pm}(\mathbf{r}_{S_{0q}}-\mathbf{r}_{S_{0q'}})}$$

$$\times \delta(\mathbf{k}^{\pm} - \mathbf{k}_{\mathrm{in}||} + \mathbf{G}_{\tilde{p}}). \tag{22}$$

Please note that this alternative formulation of the coupling operator between a grid of particles $S_{q'}$ and the central unit cell's particle S_{0q} is in general only valid if an infinite number of scattered wave vectors $\mathbf{k}^{\pm} = \mathbf{k}_{\mathrm{in}||} - \mathbf{G}_{\tilde{p}}$ are taken into account. From a practical point of view, it is recommended to be used only if $\Delta z_{S_q S_{q'}} \gg r_{S_{0q}} + r_{S_{0q'}}$. Hereby, the number of evanescent waves that have to be taken into account is strongly reduced.

Finally, we want to note that in a similar fashion to the presented direct coupling operator, the layered mediated particle-grid coupling can also be evaluated. Hereby, it becomes feasible to study periodic particle arrangements in a planar, layered environment.

3. Random, periodic particle arrangements

Recently, it has been shown that the superposition T-matrix scheme in combination with an Ewald sum approach is suitable to describe light scattering in strictly periodic particle arrangements [26, 27]. Here, we discuss its use for the simulation of random particle arrangements. First, we validate the approach by a comparison with an FEM simulation. For this purpose, we consider the periodic extent of a random, $2 \times 2 \times 2\,\mu\mathrm{m}^3$ large ensemble of pores with a $7\,\%\,(\mathrm{v}/\mathrm{v})$ volume density, embedded in a lossless material of constant refractive index of $n = 1.5$, corresponding to poly(methyl methacrylate) (PMMA). The pore radii follow a Gaussian distribution with a mean value of $107\,\mathrm{nm}$ and a standard deviation of $9\,\mathrm{nm}$. The periodic particle arrangement is excited by an x-polarized plane wave, propagating in negative z-direction. A graphical illustration of one unit cell can be found as an inset in figure 2 (a).

With a volume of $8\,\mu\mathrm{m}^3$, containing more than 100 individual scatterers, the example is chosen to pose a considerable
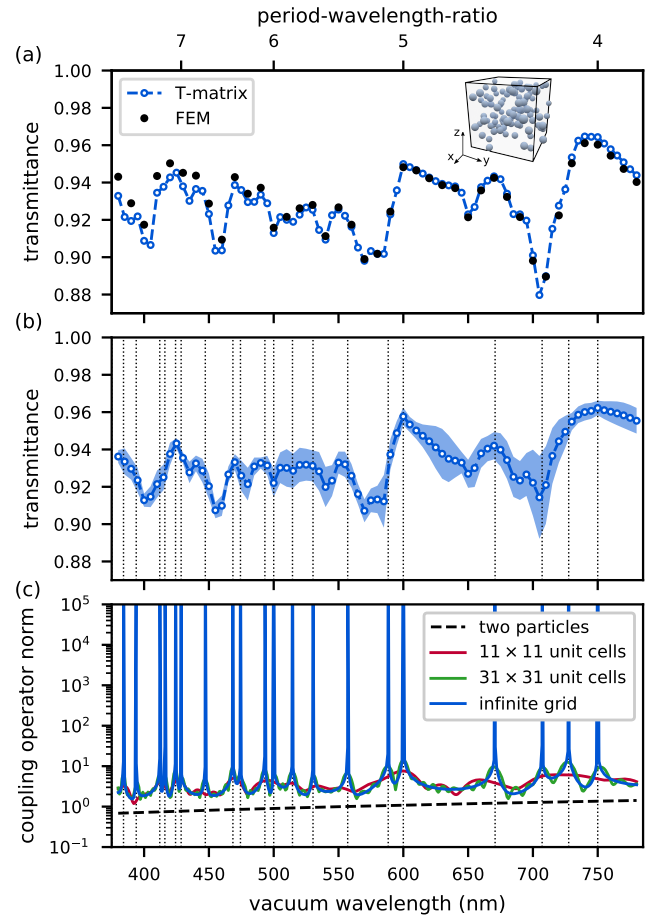
Figure 2: (a) Wavelength dependent transmittance of an x-polarized plane wave, exciting a periodic pore structure under normal incidence. The cubic unit cell has a volume of $2 \times 2 \times 2\,\mu\mathrm{m}^3$. Comparison between the periodic T-matrix scheme and the FEM. (b) Transmittance averaged over five independent particle arrangements. (c) L^2-norm of the coupling operator between a single particle and its own periodic repetition $\mathbf{W}^{S_{0q}S_q}$, for an infinite periodic grid (Ewald sum) as well as finite sized grids (direct sum of the translation operator for SVWFs). In comparison, a pair of two particles with a $2\,\mu\mathrm{m}$ displacement.

challenge to the FEM. Figure 2 (a) shows the plane wave's wavelength dependent transmittance over the visible spectrum for both, the T-matrix simulations (blue) and the results obtained with the commercially available COMSOL MULTIPHYSICS software (black) [44]. In this example each particle's T-matrix has been considered up to a maximal multipole degree and order $l_{\max} = m_{\max} = 4$. FEM simulations have been performed with a minimal spatial discretization of $0.6\,\mathrm{nm}$. Overall, we obtain a very good agreement between both techniques. A slight offset towards shorter wavelengths indicates that in this part of the spectrum, our FEM mesh does not sufficiently discretize the simulation domain. However, the immense hardware requirements related to these specific FEM simulations prevent us from using an even finer mesh. For slightly more coarse discretizations we observed larger offsets be-

5
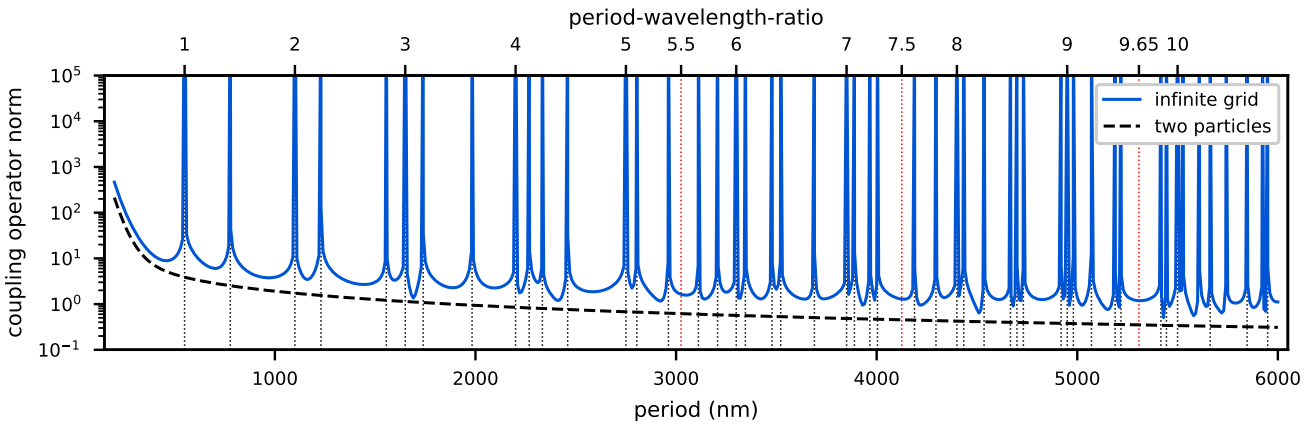
Figure 3: L^2-norm of the coupling operator between particles ($n = 2$) in vacuum, excited by a plane wave ($\lambda_0 = 550\,\text{nm}$) that is propagating perpendicular to the particle displacement. Comparison between two individual scatterers (translation addition operator for SVWFs) and an infinite periodic lattice (Ewald sum) as a function of the displacement/periodicity.

tween both simulation techniques. Yet, the overall trend remained identical.

Please note, that all 81 T-matrix simulations in figure 2 (a) have been performed on a regular work station within a single day, which is comparable to the time that each single FEM simulation occupied one node of the bwUni-Cluster 2.0.

Comparing the observed wavelength dependency to the almost linear trends that have been measured for comparable porous polymer layers [45], it remains questionable to which extent the observed quantities are influenced by the specific particle arrangements and the artificial periodicity. Therefore, we repeat the T-matrix simulations with multiple random particle configurations, keeping the periodicity fixed at $2\,\mu\text{m}$. An average of five independent configurations can be seen in figure 2 (b). Its standard deviation is denoted by a blue corridor. Independent of the individual random realization, the transmittance remains strongly dependent on the excitation wavelength. Hereby indicating that the wavelength dependent features do arise from the chosen periodicity and not from the specific implementation of the random structure.

To highlight this point, figure 2 (c) visualizes the periodicity's wavelength dependent influence on the particle-grid coupling in form of the L^2-norm of the coupling operator (eq. (9)) between an arbitrary central particle and its own infinite periodic repetition. The coupling matrix norm shows an ever increasing density of resonances towards larger period-to-wavelength ratios. From a mathematical point of view, these resonances arise from

$$\Gamma^{-1}_{\mathbf{k}_{\text{in}||}+\mathbf{G}_{\tilde{p}}} = \left(\sqrt{k^2 - (\mathbf{k}_{\text{in}||} + \mathbf{G}_{\tilde{p}})^2} \right)^{-1} \qquad (23)$$

in the long range contribution of the Ewald sum (cf. (B.3)), which leads to a singularity whenever the wave number coincides with the sum of the initial field's in-plane wave vector and the reciprocal lattice vector. As a result, one observes a strongly increased coupling

between particles within one grid, but also to particles in displaced grids (eqs. (B.6) and (B.7)). These artificial singularities have to be avoided when using Ewald's method, as they constitute a clear artifact of the periodic approximation of the otherwise aperiodic structure. However, the formation of resonances can already be observed for finite sized particle grids (11 by 11 unit cells in red, 31 by 31 unit cells in green, evaluated by direct summation of the individual particles' contributions, cf. figure 2 (c)), indicating that the resonant particle coupling does not arise from a mathematical misfeature in the Ewald sum. It can be explained by interference in an infinite periodic grid without background absorption.

For now, we conclude that introducing an artificial periodicity to model large, random particle arrangements results in artificial resonances. And while the general assumption is true that choosing a larger periodicity results in weaker particle-grid coupling (cf. figure 3), it cannot be chosen large enough to diminish any resonant behavior. Therefore, it is not sufficient to simply choose the largest period that can be handled in terms of computational resources. Instead, we propose to chose a period that in combination with the excitation wavelength and incident angle results in non-resonant coupling between a particle and a particle grid.

Considering the previously discussed example of a plane wave impinging onto a porous polymer at a given incident angle, this can be achieved by fixing the ratio between the excitation wavelength and the artificial period to obtain a detrimental, yet constant influence of the periodicity over all wavelengths. The result can be seen in figure 4 (a) for a constant period-wavelength-ratio P/λ of 9.65 (blue) in comparison to a constant period P of $2\,\mu\text{m}$ (grey, identical to figure 2 (b)). Figure 4 (b) displays the observed transmittance for different period-wavelength-ratios of 5.5, 7.5 and 9.65. These ratios between the excitation wavelength and the unit cell's period are again somewhat arbitrary

6
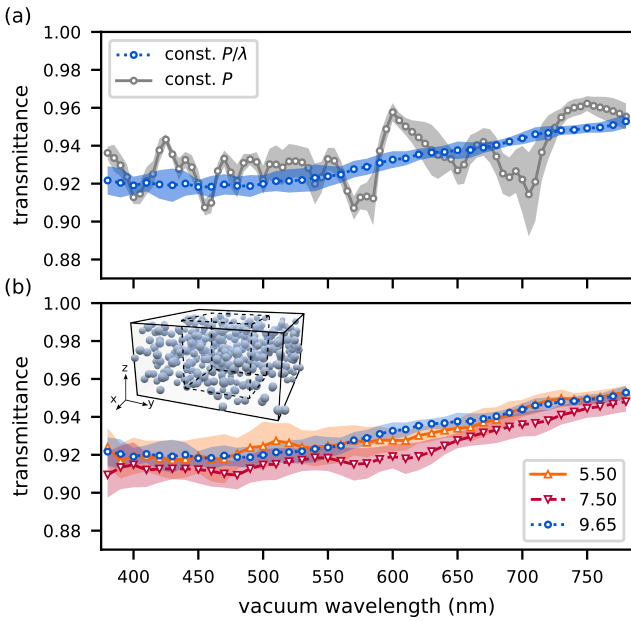
Figure 4: Average transmittance of TE- and TM-polarized plane waves exciting periodic, $2\,\mu m$ thick porous polymer films. (a) Comparison between a constant period-wavelength-ratio $P/\lambda = 9.65$ (in a homogeneous environment of $n = 1.5$) and a constant period of $2\,\mu m$. (b) Comparison between constant P/λ of 5.5, 7.5 and 9.65. The inset shows a graphical representation of the wavelength dependent unit cells for $P/\lambda = 7.5$ (smallest and largest).

but in clear distance to the neighboring singularities (see also dotted red lines in figure 3).

It remains open to which extent a further increase of the period-wavelength-ratio would lead to convergence of any observable quantity, given that P/λ is chosen in a clear distance to any neighboring singularity. However, the results reveal only minor differences for period-wavelength-ratios between 5.5 and 9.65. In addition, the transmittance' standard deviations, averaged over all wavelengths, decrease from $0.74\,\%$ to $0.69\,\%$ and $0.45\,\%$, suggesting a decaying influence of the individual particle arrangements for an increasing unit cell size.

All observed quantities have been averaged over ten independent particle arrangements. Each is constructed by sequentially populating a unit cell with random particle positions until the desired volume fraction is reached. To keep the period-wavelength-ratio constant, each excitation wavelength requires a different unit cell size. However, the particle positioning has been done only for the largest unit cells needed. For shorter wavelengths, the decreased periods have been realized by choosing the respective subdomain as a unit cell. Hereby, it may become necessary to remove particles from the unit cell boundaries if the periodicity is disrupted by overlapping particles. Inevitably, this leads to small particle density fluctuations between individual simulations. Yet, it ensures that for similar wavelengths almost identical particle arrangements are modeled. A graphical illustration of the
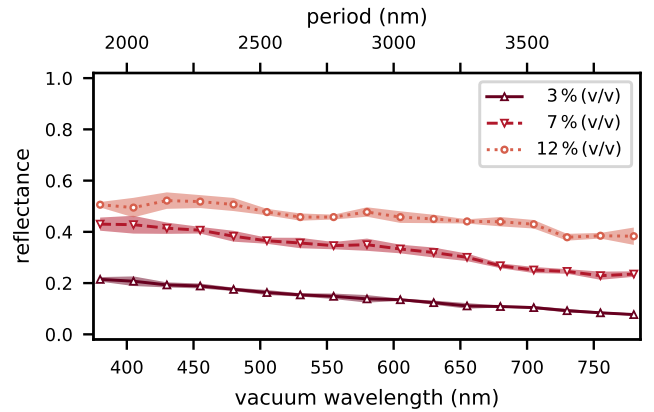
Figure 5: Average reflectance of TE- and TM-polarized plane waves by periodic, $10\,\mu m$ thick porous polymer films. Comparison between three samples of different pore sizes and densities.

wavelength dependent unit cells is shown as an inset of figure 4 (b).

4. Application example: Reflectance spectra of porous network morphologies

Finally, we would like to illustrate the capabilities of the presented approach by studying the wavelength dependent reflectance of a plane wave by $10\,\mu m$ thick porous polymer layers for three different pore sizes and densities. A graphical illustration of such structures is shown in figure 1.

Especially the case of light propagation in thick, non-absorbing particle arrangements renders an enormous challenge for many simulation techniques. Due to the finite size of non-periodic configurations, a quantitative prediction of, e.g., transmittance and reflectance can only be made if the lateral extent measures a multitude of the horizontal dimension. Otherwise it is to be expected that a considerable amount of light escapes through the lateral boundaries of the particle arrangement. Therefore, the number of particles necessary for the non-periodic case scales with the third power of the ensemble thickness. In the periodic case, it only scales linearly with the thickness, reducing the simulation time such that their numerical treatment becomes feasible.

For our example, we choose pore sizes and densities that are inspired by porous network morphologies obtained from foamed micro PMMA spheres. To reproduce the characteristic pore size distributions, we assume pore radii that follow Gaussian distributions around $90\,nm$, $107\,nm$ and $133\,nm$ with standard deviations of $7.8\,nm$, $8.9\,nm$ and $9.7\,nm$ and form networks of $3\,\%\,(v/v)$, $7\,\%\,(v/v)$ and $12\,\%\,(v/v)$ pore density, respectively.

The reflectance of a plane wave under normal incidence by these $10\,\mu m$ thick porous polymer layers is displayed in figure 5. Here, the constant period-wavelength-ratio P/λ

was set to 7.5. Each average has been taken over five individual pore configurations and their standard deviations are denoted by red corridors. Although we obtain the typically observed, almost linear wavelength dependency for all three films, stronger deviations between individual particle arrangements occur at lower wavelengths and increasing particle sizes and densities. This indicates an increased importance of the individual particle constellations for samples with stronger scattering and underlining the importance of sample averaging for such simulations.

5. Conclusions

We have shown that the superposition T-matrix scheme in combination with an Ewald sum approach to account for particle coupling in periodic particle arrangements is a powerful tool to study light propagation in large, random structures. Introducing such an artificial periodicity can lead to resonant coupling between a single particle and a particle's periodic extent. Contrary to common expectations, these resonances cannot be avoided by choosing ever increasing periodicities. However, resonant particle coupling only appears for specific combinations of the periodicity and the excitation's wave number and incident angle. Therefore, it is possible to perform parameter studies by avoiding any resonances.

The approach has been demonstrated by modeling light propagation in porous polymer layers of $10\,\mu m$ thickness. In this study, some unit cells contained more than 2000 individual scatterers.

Utilizing our modified T-matrix scheme, simulations of electromagnetic scattering in large, random particle arrangements can be performed for dielectric as well as metal particles of various shapes.

For now, the approach is only available for plane wave excitation but might be extended to periodic dipole arrays by converting the dipoles' periodic spherical waves into a finite sum of propagating plane waves in the same fashion it is done to evaluate the near-field of periodic scatterers.

Appendix A. Wave functions

All T-matrix simulations have been performed on the basis of SMUTHI [46], a python package that allows to study "scattering by multiple particles in thin-film systems". We summarize the therein used definitions and conventions necessary for section 2.

In the cylindrical coordinates $\kappa, \alpha, \pm k_z$ of wave vector $\mathbf{k}^\pm$, the plane vector wave functions read

$$\mathbf{\Phi}_j^\pm(\kappa, \alpha; \mathbf{r}) = e^{i\mathbf{k}^\pm \mathbf{r}} \hat{\mathbf{e}}_j^\pm. \tag{A.1}$$

The plus and minus sign correspond to waves propagating in positive and negative z direction, respectively. Denoted by index j (TE = 1 and TM = 2), a plane wave's polarization is defined by the unit vectors $\hat{\mathbf{e}}_1 = \hat{\mathbf{e}}_\alpha$ of the azimuthal and $\hat{\mathbf{e}}_2 = \hat{\mathbf{e}}_\beta$ of the polar angle of $\mathbf{k}^\pm$.

The spherical vector wave functions read [38]

$$\mathbf{M}_{lm1}^{(\nu)}(\mathbf{r}) = \frac{1}{\sqrt{2l(l+1)}} \nabla \times \left[\mathbf{r} z_l^{(\nu)}(kr) Y_{lm}(\theta, \varphi) \right], \tag{A.2}$$

$$\mathbf{M}_{lm2}^{(\nu)}(\mathbf{r}) = \frac{1}{k} \nabla \times \mathbf{M}_{lm1}^{(\nu)}(\mathbf{r}), \tag{A.3}$$

with the spherical coordinates θ, ϕ, r of position vector $\mathbf{r}$. In case of regular waves ($\nu = 1$), the radial wave function $z_l^{(\nu)}$ stands for the spherical Bessel functions, $z_l^{(1)} = j_l$, while outgoing waves ($\nu = 3$) involve the spherical Hankel function of first kind, $z_l^{(3)} = h_l^{(1)}$. The spherical harmonics $Y_{lm}(\theta, \varphi) = P_l^{|m|}(\cos\theta) e^{im\varphi}$ are based on the normalized associated Legendre functions $P_l^{|m|}$. For simplicity, we subsume the spherical waves multipole degree l, order m and polarization τ in a single index $n = (l, m, \tau)$.

Appendix A.1. Transformations and translations

Plane waves can be expressed in terms of regular spherical waves [47]

$$\mathbf{\Phi}_j^\pm(\kappa, \alpha; \mathbf{r}) = 4 \sum_n e^{-im\alpha} B_{nj}^\dagger \left(\pm \frac{k_z}{k} \right) \mathbf{M}_n^{(1)}(\mathbf{r}), \tag{A.4}$$

and outgoing spherical waves in plane waves

$$\mathbf{M}_n^{(3)}(\mathbf{r}) = \frac{1}{2\pi} \sum_{j=1}^2 \int \frac{d^2\mathbf{k}_{||}}{k_z k} e^{im\alpha} B_{nj} \left(\pm \frac{k_z}{k} \right) \mathbf{\Phi}_j^\pm(\kappa, \alpha; \mathbf{r}) \tag{A.5}$$

for $z \gtrless 0$.

An explicit formulation of the transformation operators B

and $B^\dagger$ can be found in [16].

While for plane waves a translation results in a simple phase shift, the translation of SVWFs is accounted for by the translation addition theorem [48]

$$\mathbf{M}_n^{(3)}(\mathbf{r} + \mathbf{d}) = \sum_{n'} A_{nn'}(\mathbf{d})\mathbf{M}_{n'}^{(1)}(\mathbf{r}), \quad |\mathbf{r}| < |\mathbf{d}| \quad (A.6)$$

with

$$A_{nn'}(\mathbf{d}) = \delta_{\tau\tau'}A_{lml'm'}(\mathbf{d}) + (1 - \delta_{\tau\tau'})B_{lml'm'}(\mathbf{d}). \quad (A.7)$$

The translation operator $A(\mathbf{d})$ can be constructed via recurrence formulas given in [13, 38] or based on the Wigner-3j symbols [37, 38, 49]. In the latter case, the translation operator reads [37]

$$A_{lml'm'}(\mathbf{d}) = \mathrm{e}^{\mathrm{i}(m-m')\varphi_d} \sum_{\lambda=|l-l'|}^{|l+l'|} a_5(l,m|l',m'|\lambda)$$
$$\times h_\lambda^{(1)}(kd)P_\lambda^{|m-m'|}(\cos\theta_d), \quad (A.8)$$

or

$$B_{lml'm'}(\mathbf{d}) = \mathrm{e}^{\mathrm{i}(m-m')\varphi_d} \sum_{\lambda=|l-l'|}^{|l+l'|} b_5(l,m|l',m'|\lambda)$$
$$\times h_\lambda^{(1)}(kd)P_\lambda^{|m-m'|}(\cos\theta_d), \quad (A.9)$$

with a_5 and b_5 being adjusted to the here used normalization conventions. Their explicit formulation can be found in [16].

Appendix B. Ewald sum

Derived by Kambe [28, 29] for the use in low energy electron diffraction theory, the quantity D_{LM} can be split into two equally fast converging sums, one for the nearfield interaction and one for long range contributions

$$D_{LM}^* = D_{LM}^{(1)} + D_{LM}^{(2)} + \delta_{L0}\delta_{M0}D_{00}^{(3)}. \quad (B.1)$$

D_{LM} can be used to evaluate the coupling between a single particle and periodic particle arrangements. Recent formulations of D_{LM} for periodic T-matrix simulations can be found in [26, 27]. For completeness, we summarize formulas of D_{LM} for various particle-grid constellations. For this purpose, we stick to the nomenclature in [26]. But please note that a normalization factor is necessary to match the definition of the SVWFs used throughout this work.

$$D_{LM} = \sqrt{2\pi} \begin{cases} (-1)^{-M} & D_{LM}^* \quad M > 0 \\ 1 & M \leq 0 \end{cases} \quad (B.2)$$

For the coupling between a particle and its own periodic grid, the long range contribution reads

$$D_{LM}^{(1)} = \frac{i^M}{(2k)^L} \frac{\sqrt{(2L+1)(L-M)!(L+M)!}}{Ak} \sum_{\tilde{p}} \mathrm{e}^{\mathrm{i}M\varphi_{\mathbf{k}_{\mathrm{in}||}+\mathbf{G}_{\tilde{p}}}}$$
$$\times \sum_{\lambda=0}^{\frac{L-|M|}{2}} \frac{(\Gamma_{\mathbf{k}_{\mathrm{in}||}+\mathbf{G}_{\tilde{p}}})^{2\lambda-1}|\mathbf{k}_{\mathrm{in}||}+\mathbf{G}_{\tilde{p}}|^{L-2\lambda}}{\lambda!(\frac{L+M}{2}-\lambda)!(\frac{L-M}{2}-\lambda)!}$$
$$\times \Gamma\left(\frac{1}{2} - \lambda, -\frac{\Gamma_{\mathbf{k}_{\mathrm{in}||}+\mathbf{G}_{\tilde{p}}}^2}{4\eta^2}\right), \quad (B.3)$$

and the short range contribution

$$D_{LM}^{(2)} = (-i)(-1)^{\frac{L+M}{2}} \frac{\sqrt{(2L+1)(L-M)!(L+M)!}}{2^{L+1}\pi(\frac{L-M}{2})!(\frac{L+M}{2})!}$$
$$\times \sum_{p' \neq 0} \mathrm{e}^{\mathrm{i}\mathbf{k}_{\mathrm{in}||}\mathbf{R}_{p'}} \mathrm{e}^{\mathrm{i}M\varphi_{-R_{p'}}} \frac{1}{k}\left(\frac{2|\mathbf{R}_{p'}|}{k}\right)^L$$
$$\times \int_{\eta^2}^{\infty} u^{L-\frac{1}{2}} \mathrm{e}^{-|\mathbf{R}_{p'}|^2 u + \frac{k^2}{4u}} du. \quad (B.4)$$

Note that for $L+M$ odd, the Ewald sum vanishes. In case of $L = M = 0$, a central particle correction is necessary

$$D_{00}^{(3)} = \frac{1}{4\pi}\Gamma\left(-\frac{1}{2}, -\frac{k^2}{4\eta^2}\right). \quad (B.5)$$

$\varphi_{\mathbf{k}_{\mathrm{in}||}+\mathbf{G}_{\tilde{p}}}$ denotes the azimuthal angle of the linear combination of the initial in-plane wave vector $\mathbf{k}_{\mathrm{in}||}$ and the reciprocal lattice vector $\mathbf{G}_{\tilde{p}}$ and $\Gamma_{\mathbf{k}_{\mathrm{in}||}+\mathbf{G}_{\tilde{p}}} = \sqrt{k^2 - (\mathbf{k}_{\mathrm{in}||} + \mathbf{G}_{\tilde{p}})^2}$ with positive complex square root convention. $\Gamma(\cdot,\cdot)$ denotes the upper incomplete gamma function and η the separation parameter between real and reciprocal space summation.

If the coupling between a particle and another particle's periodic repetition is demanded, one has to distinguish between particles within the same xy-plane ($c_z = 0$) and particles at different z positions [29]. In the former case the long range contribution reads

$$D_{LM}^{(1)} = \frac{i^M}{(2k)^L} \frac{\sqrt{(2L+1)(L-M)!(L+M)!}}{Ak}$$
$$\times \sum_{\tilde{p}} \mathrm{e}^{-\mathrm{i}(\mathbf{k}_{\mathrm{in}||}+\mathbf{G}_{\tilde{p}})\mathbf{c}} \mathrm{e}^{\mathrm{i}M\varphi_{\mathbf{k}_{\mathrm{in}||}+\mathbf{G}_{\tilde{p}}}}$$
$$\times \sum_{\lambda=0}^{\frac{L-|M|}{2}} \frac{(\Gamma_{\mathbf{k}_{\mathrm{in}||}+\mathbf{G}_{\tilde{p}}})^{2\lambda-1}|\mathbf{k}_{\mathrm{in}||}+\mathbf{G}_{\tilde{p}}|^{L-2\lambda}}{\lambda!(\frac{L+M}{2}-\lambda)!(\frac{L-M}{2}-\lambda)!}$$
$$\times \Gamma\left(\frac{1}{2} - \lambda, -\frac{\Gamma_{\mathbf{k}_{\mathrm{in}||}+\mathbf{G}_{\tilde{p}}}^2}{4\eta^2}\right). \quad (B.6)$$

If $c_z \neq 0$,

$$
\begin{aligned}
D_{LM}^{(1)} &= \frac{(-i)^M}{(-2)^L} \frac{\sqrt{(2L+1)(L-M)!(L+M)!}}{Ak^2} \\
&\times \sum_{\tilde{p}} e^{-i(\mathbf{k}_{\text{in}||}+\mathbf{G}_{\tilde{p}})\mathbf{c}} e^{iM\varphi_{\mathbf{k}_{\text{in}||}+\mathbf{G}_{\tilde{p}}}} \\
&\times \sum_{n=0}^{L-|M|} \left(\frac{\Gamma_{\mathbf{k}_{\text{in}||}+\mathbf{G}_{\tilde{p}}}}{k}\right)^{2n-1} \Delta_n \\
&\times \sum_{s=n}^{\min(L-|M|,2n)} \frac{(-kc_z)^{2n-s} \left(\frac{|\mathbf{k}_{\text{in}||}+\mathbf{G}_{\tilde{p}}|}{k}\right)^{L-s}}{(2n-s)!(s-n)! \left(\frac{L+|M|-s}{2}\right)! \left(\frac{L-|M|-s}{2}\right)!}.
\end{aligned}
\tag{B.7}
$$

In both cases the short range contribution reads

$$
\begin{aligned}
D_{LM}^{(2)} &= -i\sqrt{\frac{2}{\pi}} \sum_{p'} e^{i\mathbf{k}_{\text{in}||}\mathbf{R}_{p'}} (k|\mathbf{R}_{p'}+\mathbf{c}|)^L Y_{LM}^*(-\mathbf{R}_{p'}-\mathbf{c}) \\
&\times \int_{\eta^2}^{\infty} u^{2L} e^{-\frac{(k|\mathbf{R}_{p'}+\mathbf{c}|)^2 u^2}{2}+\frac{1}{2u^2}} \, du.
\end{aligned}
\tag{B.8}
$$

Recursion formulas for the integral Δ_n, as well as for the integrals in eqs. (B.4) and (B.8) and the upper incomplete gamma function are provided by Kambe [28, 29].

Please note that in the case of unit cells much larger than the wavelength, the separation parameter η has to be chosen with care. In contrast to the optimal choice for small unit cells ($\eta = \pi/A_{\text{uc}}$) [50, 51], one operates in a regime beyond the so called high-frequency breakdown. Here, it is necessary to regulate the exponential growth in the upper incomplete gamma function to ensure convergence [27].

References

[1] P. Vukusic, B. Hallam, J. Noyes, Brilliant whiteness in ultrathin beetle scales, Science 315 (5810) (2007) 348. doi:10.1126/science.1134666.

[2] S. Vignolini, B. Glover, U. Steiner, Photonic structures in plants, Biomimetics in Photonics (2012) 1–17doi:10.1201/b13067.

[3] B. Fritz, R. Hünig, R. Schmager, M. Hetterich, U. Lemmer, G. Gomard, Assessing the influence of structural disorder on the plant epidermal cells' optical properties: A numerical analysis, Bioinspiration and Biomimetics 12 (3) (2017). doi:10.1088/1748-3190/aa6c46.

[4] P. D. García, R. Sapienza, Á. Blanco, C. López, Photonic glass: A novel random material for light, Adv. Mater. 19 (18) (2007) 2597–2602. doi:10.1002/adma.200602426.

[5] G. Shang, L. Maiwald, H. Renner, D. Jalas, M. Dosta, S. Heinrich, A. Petrov, M. Eich, Photonic glass for high contrast structural color, Sci. Rep. 8 (1) (2018) 1–9. doi:10.1038/s41598-018-26119-8.

[6] Y. Li, M. Kovacic, J. Westphalen, S. Oswald, Z. Ma, C. Hänisch, P.-A. Will, L. Jiang, M. Junghaehnel, R. Scholz, S. Lenk, S. Reineke, Tailor-made nanostructures bridging chaos and order for highly efficient white organic light-emitting diodes, Nat. Commun. 10 (1) (2019) 2972. doi:10.1038/s41467-019-11032-z.

[7] Y. J. Donie, D. Theobald, S. Moghadamzadeh, A. Mertens, I. M. Hossain, U. W. Paetzold, U. Lemmer, G. Gomard, Planarized and Compact Light Scattering Layers Based on Disordered Titania Nanopillars for Light Extraction in Organic Light Emitting Diodes, Adv. Opt. Mater. 2001610 (2020) 2001610. doi:10.1002/adom.202001610.

[8] Z. Fang, H. Zhu, Y. Yuan, D. Ha, S. Zhu, C. Preston, Q. Chen, Y. Li, X. Han, S. Lee, G. Chen, T. Li, J. Munday, J. Huang, L. Hu, Novel Nanostructured Paper with Ultrahigh Transparency and Ultrahigh Haze for Solar Cells, Nano Lett. 14 (2) (2014) 765–773. doi:10.1021/nl404101p.

[9] M. Burresi, F. Pratesi, F. Riboli, D. S. Wiersma, Complex Photonic Structures for Light Harvesting, Adv. Opt. Mater. 3 (6) (2015) 722–743. doi:10.1002/adom.201400514.

[10] S. Mühlig, C. Rockstuhl, V. Yannopapas, T. Bürgi, N. Shalkevich, F. Lederer, Optical properties of a fabricated self-assembled bottom-up bulk metamaterial, Opt. Express 19 (10) (2011) 9607. doi:10.1364/OE.19.009607.

[11] A. Rahimzadegan, D. Arslan, R. N. S. Suryadharma, S. Fasold, M. Falkner, T. Pertsch, I. Staude, C. Rockstuhl, Disorder-Induced Phase Transitions in the Transmission of Dielectric Metasurfaces, Phys. Rev. Lett. 122 (1) (2019) 015702. doi:10.1103/PhysRevLett.122.015702.

[12] B. Peterson, S. Ström, T matrix for electromagnetic scattering from an arbitrary number of scatterers and representations of E(3), Phys. Rev. D 8 (10) (1973) 3661–3678. doi:10.1103/PhysRevD.8.3661.

[13] D. A. Mackowski, Analysis of Radiative Scattering for Multiple Sphere Configurations, Proc. Math. Phys. Sci. 433 (1889) (1991) 599–614.

[14] C. Etrich, S. Fahr, M. Hedayati, F. Faupel, M. Elbahri, C. Rockstuhl, Effective Optical Properties of Plasmonic Nanocomposites, Materials (Basel). 7 (2) (2014) 727–741. doi:10.3390/ma7020727.

[15] F. Utel, L. Cortese, D. S. Wiersma, L. Pattelli, Optimized White Reflectance in Photonic-Network Structures, Adv. Opt. Mater. 7 (18) (2019) 1900043. doi:10.1002/adom.201900043.

[16] A. Egel, L. Pattelli, G. Mazzamuto, D. S. Wiersma, U. Lemmer, CELES: CUDA-accelerated simulation of electromagnetic scattering by large ensembles of spheres, J. Quant. Spectrosc. Radiat. Transf. 199 (2017) 103–110. doi:10.1016/j.jqsrt.2017.05.010.

[17] D. Werdehausen, X. G. Santiago, S. Burger, I. Staude, T. Pertsch, C. Rockstuhl, M. Decker, Modeling Optical Materials at the Single Scatterer Level: The Transition from Homogeneous to Heterogeneous Materials, Adv. Theory Simulations 3 (11) (2020) 2000192. doi:10.1002/adts.202000192.

[18] J. Markkanen, A. J. Yuffa, Fast superposition T-matrix solution for clusters with arbitrarily-shaped constituent particles, J. Quant. Spectrosc. Radiat. Transf. 189 (2017) 181–188.

[19] W. Lamb, D. M. Wood, N. W. Ashcroft, Long-wavelength electromagnetic propagation in heterogeneous media, Phys. Rev. B 21 (6) (1980) 2248–2266. doi:10.1103/PhysRevB.21.2248.

[20] A. Liebsch, B. N. J. Persson, Optical properties of small metallic particles in a continuous dielectric medium, J. Phys. C Solid State Phys. 16 (27) (1983) 5375–5391. doi:10.1088/0022-3719/16/27/019.

[21] A. Modinos, Scattering of electromagnetic waves by a plane of spheres-formalism, Phys. A Stat. Mech. its Appl. 141 (2-3) (1987) 575–588. doi:10.1016/0378-4371(87)90184-1.

[22] N. Stefanou, A. Modinos, Scattering of light from a two-dimensional array of spherical particles on a substrate, J. Phys. Condens. Matter 3 (41) (1991) 8135–8148. doi:10.1088/0953-8984/3/41/012.

[23] N. Stefanou, A. Modinos, Scattering of electromagnetic waves by a disordered two-dimensional array of spheres, J. Phys. Condens. Matter 5 (47) (1993) 8859–8868. doi:10.1088/0953-8984/5/47/011.

[24] N. Stefanou, V. Yannopapas, A. Modinos, Heterostructures of photonic crystals: frequency bands and transmission coefficients, Comput. Phys. Commun. 113 (1) (1998) 49–77. doi:10.1016/S0010-4655(98)00060-5.

[25] N. Stefanou, V. Yannopapas, A. Modinos, MULTEM 2: A new version of the program for transmission and band-structure calculations of photonic crystals, Comput. Phys. Commun. 132 (1-

2) (2000) 189–196. doi:10.1016/S0010-4655(00)00131-4.

[26] D. Beutel, A. Groner, C. Rockstuhl, I. Fernandez-Corbaton, Efficient simulation of bi-periodic, layered structures based on the T-matrix method, arXiv (2020). arXiv:2004.08098.

[27] M. Nečada, P. Törmä, Multiple-scattering T-matrix simulations for nanophotonics: symmetries and periodic lattices, arXiv (2020) 1–43arXiv:2006.12968.

[28] K. Kambe, Theory of Low-Energy Electron diffraction: I. Application of the Cellular Method to Monatomic Layers, Zeitschrift fuer Naturforsch. 22 a (1967) 322–330.

[29] K. Kambe, Theory of Low-Energy Electron Diffraction: II. Cellular Method for Complex Monolayers and Multilayers, Zeitschrift fuer Naturforsch. 23 a (1968) 1280–1294. doi:10.1515/zna-1968-0908.

[30] B. T. Draine, P. J. Flatau, Discrete-dipole approximation for periodic targets: theory and tests, J. Opt. Soc. Am. A 25 (11) (2008) 2693. doi:10.1364/JOSAA.25.002693.

[31] D. Mackowski, Van de Hulst Essay: The DDA, the RTE, and the computation of scattering by plane parallel layers of particles, J. Quant. Spectrosc. Radiat. Transf. 189 (2017) 43–59. doi:10.1016/j.jqsrt.2016.10.007.

[32] S. Sukhov, D. Haefner, A. Dogariu, Coupled dipole method for modeling optical properties of large-scale random media, Phys. Rev. E 77 (6) (2008) 066709. doi:10.1103/PhysRevE.77.066709.

[33] D. Mackowski, B. Ramezanpour, A plane wave model for direct simulation of reflection and transmission by discretely inhomogeneous plane parallel media, J. Quant. Spectrosc. Radiat. Transf. 213 (2018) 95–106. doi:10.1016/j.jqsrt.2018.02.003.

[34] M. J. A. Ruszala, N. A. Rowson, L. M. Grover, R. A. Choudhery, Low Carbon Footprint TiO2 Substitutes in Paint: A Review, Int. J. Chem. Eng. Appl. 6 (5) (2015) 331–340. doi:10.7763/IJCEA.2015.V6.505.

[35] J. Syurik, G. Jacucci, O. D. Onelli, H. Hölscher, S. Vignolini, Bioinspired Highly Scattering Networks via Polymer Phase Separation, Adv. Funct. Mater. 28 (24) (2018) 1706901. doi:10.1002/adfm.201706901.

[36] S. Costeux, CO 2 -blown nanocellular foams, J. Appl. Polym. Sci. 131 (23) (2014) 41293. doi:10.1002/app.41293.

[37] M. I. Mishchenko, L. D. Travis, A. A. Lacis, Scattering, Absorption, and Emission of Light by Small Particles, Cambridge University Press, 2002.

[38] A. Doicu, T. Wriedt, Y. Eremin, Light Scattering by Systems of Particles, Springer, Berlin, Heidelberg, 2006. doi:10.1007/978-3-642-02646-1.

[39] A. Doicu, T. Wriedt, Extended boundary condition method with multipole sources located in the complex plane, Opt. Commun. 139 (1-3) (1997) 85–91. doi:10.1016/S0030-4018(97)00113-2.

[40] D. W. Mackowski, Discrete dipole moment method for calculation of the T matrix for nonspherical particles, J. Opt. Soc. Am. A 19 (5) (2002) 881. doi:10.1364/JOSAA.19.000881.

[41] M. Fruhnert, I. Fernandez-Corbaton, V. Yannopapas, C. Rockstuhl, Computing the T-matrix of a scattering object with multiple plane wave illuminations, Beilstein J. Nanotechnol. 8 (1) (2017) 614–626. doi:10.3762/bjnano.8.66.

[42] J. B. Pendry, Low energy electron diffraction : the theory and its application to determination of surface structure, Academic Press, 1974.

[43] D. Theobald, A. Egel, G. Gomard, U. Lemmer, Plane-wave coupling formalism for T-matrix simulations of light scattering by nonspherical particles, Phys. Rev. A 96 (3) (2017) 033822. doi:10.1103/PhysRevA.96.033822.

[44] COMSOL, Comsol Multiphysics, www.comsol.com, 2021.

[45] J. Syurik, R. H. Siddique, A. Dollmann, G. Gomard, M. Schneider, M. Worgull, G. Wiegand, H. Hölscher, Bio-inspired, large scale, highly-scattering films for nanoparticle-alternative white surfaces, Sci. Rep. 7 (1) (2017) 46637. doi:10.1038/srep46637.

[46] A. Egel, K. M. Czajkowski, D. Theobald, K. Ladutenko, A. S. Kuznetsov, L. Pattelli, SMUTHI: A python package for the simulation of light scattering by multiple particles near or between planar interfaces, arXiv (2021). arXiv:2105.04259.

[47] A. Boström, G. Kristensson, S. Ström, Transformation Properties of Plane, Spherical and Cylindrical Scalar and Vector Wave Functions, in: F. Represent. Introd. to Scatt., Elsevier Science Publishers B.V., 1991, pp. 165–210.

[48] O. R. Cruzan, Translational addition theorems for spherical vector wave functions, Q. Appl. Math. 20 (1) (1962) 33–40.

[49] S. Stein, Addition Theorems for Spherical Wave Functions, Q. Appl. Math. 19 (1) (1961) 15–24. doi:10.2144/000113897.

[50] K. E. Jordan, G. R. Richter, P. Sheng, An efficient numerical evaluation of the Green's function for the Helmholtz operator on periodic structures, J. Comput. Phys. 63 (1) (1986) 222–235. doi:10.1016/0021-9991(86)90093-8.

[51] C. M. Linton, Lattice Sums for the Helmholtz Equation, SIAM Rev. 52 (4) (2010) 630–674. doi:10.1137/09075130X.